

Reciprocal interaction between cortical SST and PV interneurons in top-down regulation of retinothalamic refinement

Qiufen Jiang^{a,b}, Sherry Jingjing Wu^{b,c}, Gord Fishell^{b,c,1}, and Chinfei Chen^{a,b,1}

Affiliations are included on p. 10.

Edited by Marla Feller, University of California Berkeley, CA; received February 26, 2025; accepted April 19, 2025

Refinement of thalamic circuits is crucial for the proper maturation of sensory circuits. In the visual system, this process is regulated by corticothalamic feedback during the experience-dependent phase of development. Yet the cortical circuits modulating this feedback remain elusive. Here, we demonstrate opposing roles for cortical somatostatin (SST) and parvalbumin (PV) interneurons in shaping retinogeniculate connectivity during the thalamic sensitive period (P20-30). Early in the refinement process, SST interneurons promote the strengthening and pruning of retinal inputs in the thalamus, as evidenced by disrupted synaptic refinement following their ablation. In contrast, PV interneurons, which mature later, act as a brake on this refinement, with their ablation leading to enhanced pruning of retinogeniculate connections. Notably, manipulating the relative balance between these inhibitory circuits can regulate sensory deprivation-induced retinogeniculate remodeling. Taken together, our findings show that cortical SST and PV interneuron circuits drive experience-dependent reciprocal antagonism that gates cortical feedback regulation of feedforward thalamic refinement.

cortical feedback | retinogeniculate synapse | SST interneurons | PV interneurons | synaptic refinement

Multiple aspects of the visual system are substantially reorganized as maturation proceeds. A key example of this is seen at the mouse retinogeniculate synapse, where the establishment of developmental circuits is followed by a second phase of refinement that is driven by sensory experience (1, 2). During this developmental window, called the thalamic sensitive period, external stimuli provide the signals for fine-tuning this connection between the eye and the visual thalamus (1-4). For instance, visual deprivation during this period, referred to as late dark rearing (LDR), leads to an increase in the number of converging retinal inputs and a decrease in the average synaptic strength of the retinogeniculate connections (1, 5). Conversely, rearing under specific patterns of visual activity increases the distribution of thalamic neurons that respond to these visual stimuli—a process that relies on proper retinogeniculate remodeling (6). In mice, this remodeling occurs between postnatal day (P)20 to P30, a process traditionally considered to be solely driven by bottom-up visual experience. Despite this canonical view, developmental studies of the visual system indicate that information during this period is far from unidirectional and that the primary visual cortex (V1) is both activated and centrally involved in bidirectional communication with the thalamus (7, 8). Multiple lines of evidence indicate that this top-down signaling plays a key role in directing the reorganization of retinogeniculate synapses (5, 8, 9). Specifically, changing the activity of cortical feedback signaling alters retinogeniculate refinement. Increasing or decreasing the activity of layer (L) six corticothalamic neurons in V1 alters retinogeniculate connectivity during the thalamic sensitive period (5), highlighting the importance of cortical-thalamic feedback in subcortical circuit refinement (10, 11). Given the need for precise coordination of cortical and thalamic maturation, a key question is how these processes are jointly regulated. How does visual experience processed within the cortex dynamically modulate top-down feedback to drive the remodeling of retinogeniculate synapses (Fig. 1A)? The precise timing during which the retinogeniculate circuits are reorganized provides a potential hint that top-down corticothalamic signals regulating this process must also be precisely controlled. As infragranular pyramidal neurons (PNs) in V1 can be significantly tuned by local interneurons (12–15), we speculated that the maturation of inhibitory circuits regulating corticothalamic cells could play a central role in coordinating cortical and thalamic

Somatostatin (SST) and parvalbumin (PV) interneurons are two major interneuron types that modulate cortical function. The developmental regulation of these two populations is critical to the shift in cortical circuits from synchronous to decorrelated activity

Significance

Proper development of retinal inputs into the thalamus is critical for sensory perception. In the visual system, sensory experience can influence the refinement of connections between the eye, thalamus, and cortex. Recent work indicates that the refinement of this process is as dependent upon top-down inputs from the cortex, as upon bottom-up signaling from the retina. In this study, we investigate how the balance of cortical inhibition from somatostatin and parvalbumin inhibitory cells plays a surprisingly central role in this refinement process. Evidence is presented demonstrating that the opposing roles of these two interneuron types in cortical regulation have a dramatic effect on thalamic circuit development. These findings uncover the importance of inhibitory circuit balance in dynamically coordinating thalamocortical maturation.

Author contributions: Q.J., G.F., and C.C. designed research; Q.J. and S.J.W. performed research; Q.J. and S.J.W. analyzed data; and Q.J., G.F., and C.C. wrote the

The authors declare no competing interest.

This article is a PNAS Direct Submission.

Copyright © 2025 the Author(s), Published by PNAS, This article is distributed under Creative Commons Attribution-NonCommercial-NoDerivatives License 4.0

¹To whom correspondence may be addressed. Email: Gordon_Fishell@hms.harvard.edu or Chinfei.Chen@

This article contains supporting information online at https://www.pnas.org/lookup/suppl/doi:10.1073/pnas. 2504224122/-/DCSupplemental.

Published June 18, 2025.

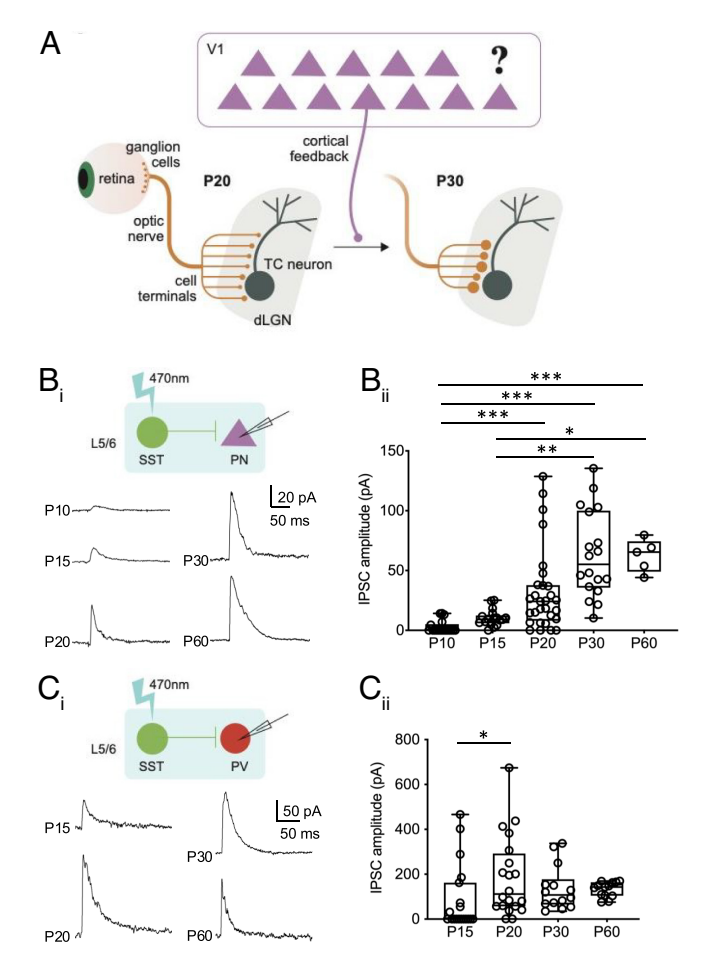


Fig. 1. Maturation of somatostatin (SST) interneuron-mediated cortical circuits during the sensitive period for thalamic plasticity. (*A*) Corticothalamic neurons in V1 L6 project to the dLGN and regulate the feedforward retinogeniculate refinement (5). (*B*) Developmental time course of inhibitory postsynaptic currents (IPSCs) from SST interneurons to PNs (SST \rightarrow PNs) in V1 L5/6. (B_{ir} , Top) Schematic of optogenetic stimulation; (Bottom) Example traces; (B_{ir}): Amplitude of SST \rightarrow PN IPSCs over development. (*C*) Similar to (*B*) but for SST \rightarrow Parvalbumin (PV) interneuron IPSCs. (B and C): *P< 0.05, *P< 0.01, **P< 0.001, Kruskal-Wallis test, Dunn's multiple comparisons test.

(14, 16–24). These developmental changes likely have a top-down effect on thalamic function regulated through corticothalamic feedback. To explore this idea, the output from SST interneurons onto PV interneurons and PNs in infragranular layers was examined in V1 using slice electrophysiology across development. Notably, the development of infragranular inhibitory circuits showed a similar sensitivity to sensory experience as retinogeniculate synapses within the same developmental time window, raising the possibility that the maturation of these inhibitory circuits influences top-down regulation of retinogeniculate refinement in the dorsal lateral geniculate nucleus (dLGN). To test this hypothesis, we manipulated the inhibitory circuits in V1 by ablating cortical SST or PV interneurons and evaluated the impact on retinogeniculate synapse refinement. Ablation of SST interneurons during the thalamic sensitive period disrupted both PV interneuron firing maturation and retinogeniculate synapse refinement. In contrast, ablation of PV interneurons during the same period enhanced retinogeniculate pruning. Moreover, activation of SST interneurons or ablation of PV interneurons during the sensitive period prevented the rewiring of retinogeniculate connections in response to visual deprivation. Taken together, our findings support a model in which SST and PV interneurons provide reciprocal antagonism to fine-tune the refinement of feedforward

thalamic circuits. Our study highlights local interneurons as key regulators of experience-dependent interactions between cortical and thalamic circuits.

Results

Connectivity of SST Interneuron Circuits Matures before the **End of Thalamic Sensitive Period.** Infragranular PNs are a major source of cortical output. In L6 of V1, PNs send abundant longrange projections to the first-order thalamus (5, 25-29) and receive local inhibitory inputs from deep-layer interneurons (15). Both SST and PV interneurons initially appear in infragranular layers during development (SI Appendix, Fig. S1 A and B) and thus are well positioned to modulate cortical feedback circuits. During the thalamic sensitive period, cortical inhibitory circuits are still undergoing developmental changes. To understand how these developing circuits impact corticothalamic feedback, we examined the functional responses of SST and PV interneuron circuits in infragranular layers of V1 from P10-60, a period spanning both eye opening at ~P14 and the thalamic sensitive period (P20-30). Due to the early onset of Sst expression, developing SST interneurons can be identified in V1 by immunolabeling at perinatal ages (e.g., embryonic day 20 in rat) (30) and can be genetically targeted using Sst-IRES-Cre line. When crossed to the Ai14 reporter line, Sst;tdTomato(tdT) mice labeled a stable population of SST interneurons from P15-30 (SI Appendix, Fig. S1 A, Top and SI Appendix, Fig. S1 B, Left). In contrast, tracking the developing PV interneurons is more challenging due to the late onset of Pvalb expression. Although PV interneurons are present in the cortex earlier (31-33), the expression of Pvalb turns on gradually between P10-30 (34). In Pvalbumin-tdTomato (PvalbtdT) transgenic mice, only a small number of PV interneurons are genetically labeled before P20 (SI Appendix, Fig. S1 A, Bottom). Between P20 and P30 the number of labeled cells increases 22-fold (SI Appendix, Fig. S1 B, Right). These labeled cells were confirmed by RNAscope in situ hybridization to be *Gad1*⁺ *Pvalb*⁺ interneurons (see Materials and Methods and SI Appendix, Fig. S1 C-F).

Since SST interneurons mature earlier than PV interneurons, we sought to characterize the developmental changes in the output circuitry of SST interneurons within infragranular layers. To achieve this, we recorded from PNs or genetically labeled PV interneurons (*Pvalb-tdT* mice) in L6 while optogenetically stimulating L5/6 SST interneurons using Sst; ChR2 mice (progeny of Sst-Cre mice crossed with Ai32, a channelrhodopsin (ChR2) reporter line) (SI Appendix, Fig. S2 A and B; see Materials and *Methods*). PNs were recorded from L6 (identified as the cortical layer no more than 200 µm dorsal to the white matter tract; see Materials and Methods) because we found that the vast majority of excitatory neurons in this layer are labeled by Tle4 (~84%), a marker for corticothalamic neurons (SI Appendix, Fig. S1 G-1) (35–37). Therefore, our PN recordings are enriched in corticothalamic neurons. Between P15 and P30 the median peak amplitude of SST→PN inhibitory postsynaptic currents (IPSCs) increases and plateaus (Fig. 1B and SI Appendix, Table S1). In contrast, the strengthening of the SST→PV synapse stabilizes earlier, around P20 (Fig. 1C and SI Appendix, Table S2). The changes in SST synaptic charge transfer onto PN and PV interneurons over time, measured as the integral of the synaptic waveform, align with the observed amplitude changes (SI Appendix, Fig. S2 C and D). Therefore, by the end of the thalamic sensitive period, the infragranular inhibitory circuits mediated by SST interneurons have matured in V1, with the strengthening of SST→PV connection (P15-P20) occurring within the broader developing window of SST→PN development (P15-P30).

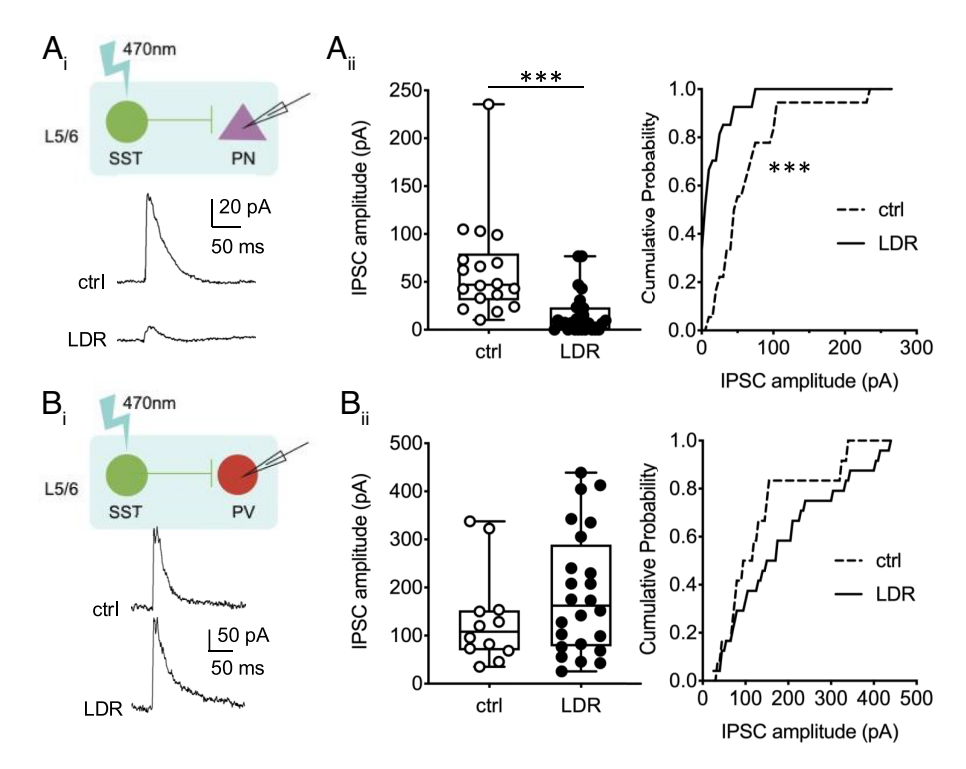


Fig. 2. The maturation of SST interneuron-mediated circuits is regulated by LDR. (A) Effect of LDR on P30 SST \rightarrow PN IPSCs. (A_j): Example traces; (A_{jj}, Left) Peak amplitudes of SST→PN IPSCs, ***P < 0.001, Mann–Whitney test; (A_{ji}, Right) Cumulative probability distribution of SST→PN IPSC amplitude, ***P < 0.001, Kolmogorov– Smirnov test. (B) Effect of LDR on P30 SST \rightarrow PV IPSCs. (B_{ij}): Example traces; (B_{ij}, Left) Peak amplitudes of SST \rightarrow PV IPSCs. There is no significant difference in the distribution or variance between ctrl and LDR groups. P = 0.224, Mann–Whitney test; P = 0.392, F test; $(B_{ij}, Right)$ Cumulative probability distribution of SST \rightarrow PV IPSC amplitude, P = 0.336, Kolmogorov–Smirnov test.

Maturation of SST Synaptic Circuits in V1 Is Regulated by Visual **Experience after Eye-Opening.** Previous studies have shown that visual deprivation of mice between P20 and P30 (LDR), a significant change in sensory experience, triggers substantial rewiring of retinogeniculate connectivity, characterized by an increase in the number of retinal ganglion cell inputs onto a thalamocortical (TC) neuron and a decrease in the average strength of these inputs (1, 2). If cortical interneurons actively participate in the process of experience-dependent retinogeniculate refinement by modulating corticothalamic feedback, we hypothesized that LDR also impacts the development of these inhibitory circuits. To test this, we examined the inhibitory outputs from SST interneurons, including SST-PN and SST-PV synapses in L5/6 of V1 after LDR (Fig. 2), at a time point when inhibitory circuits have normally matured under standard light/dark conditions. The median amplitude of SST→PN IPSCs in LDR mice is significantly reduced (Fig. 2 A_{ii} , Left and SI Appendix, Table S1), and their cumulative probability curve is shifted to smaller amplitudes compared to controls reared in normal 12-h light/dark cycles (NR, Fig. 2 Aip, Right). Notably, the strength of SST→PN synapses in LDR mice is reduced to a level comparable to that seen in P15 NR mice (P = 0.83, Mann–Whitney test), which is lower than the median strength observed at the onset of LDR in P20 NR mice (P < 0.05, Mann-Whitney test). In contrast, the amplitude of SST→PV IPSCs shows no significant changes after LDR (Fig. 2B and SI Appendix, Table S2). Therefore, inhibition from infragranular SST interneurons to PNs is sensitive to sensory experience during the thalamic sensitive period.

Ablation of SST Interneurons during Development Disrupts Pruning and Strengthening of Retinogeniculate Synapses. Our findings that SST interneuron-mediated circuits mature concurrently with retinogeniculate refinement, and exhibit similar

sensitivity to sensory experience, suggest a potential role for these cortical interneurons in influencing thalamic circuit development. To test this hypothesis, we selectively ablated SST interneurons by injecting Cre-dependent Caspase3 (Casp3)-expressing virus into V1 of Sst;tdT or Sst;ChR2 mice at P15 and assessed changes in retinogeniculate connectivity 15 to 20 d later (Fig. 3A). By P30, the majority of SST interneurons are eliminated across all cortical layers (Fig. 3B), resulting in a significant weakening of L5/6 SST \rightarrow PN and SST \rightarrow PV synapses (Fig. 3 C and D and SI Appendix, Tables S1 and S2). We then examined the effects of ablating SST interneurons on the refinement of retinogeniculate synapses by recording excitatory postsynaptic currents (EPSCs) from TC neurons in the dLGN using slice electrophysiology (Fig. $3E_i$) (1, 2). Two parameters were used to assess synaptic refinement. First, single fiber (SF) strength quantifies the magnitude of the average retinal input onto a TC neuron. Second, the fiber fraction (FF), calculated as peak SF EPSC amplitude/ maximum EPSC amplitude, measures the contribution of a single retinal input to total retinal drive, which estimates the degree of retinal input pruning. In normal development, retinogeniculate refinement leads to an increase in both FF and SF, where a higher FF indicates a reduction of converging retinal inputs due to pruning, while a greater SF reflects an increase in synaptic strength (Materials and Methods). When compared to control mice, both the maximum retinal EPSCs and SF EPSCs are significantly weaker in mice ex pressing Casp3 in V1 SST interneurons (Fig. 3 E_{ii} and E_{iii} and SI Appendix, Table S3). The FF is also significantly reduced (Fig. $3E_{iv}$ and *SI Appendix*, Table S3), consistent with an increase in the number of convergent retinal inputs innervating each TC neuron (1). Taken together, these results demonstrate that eliminating cortical SST interneurons leads to reduced retinogeniculate synaptic strength and pruning, consistent with a less refined connection.

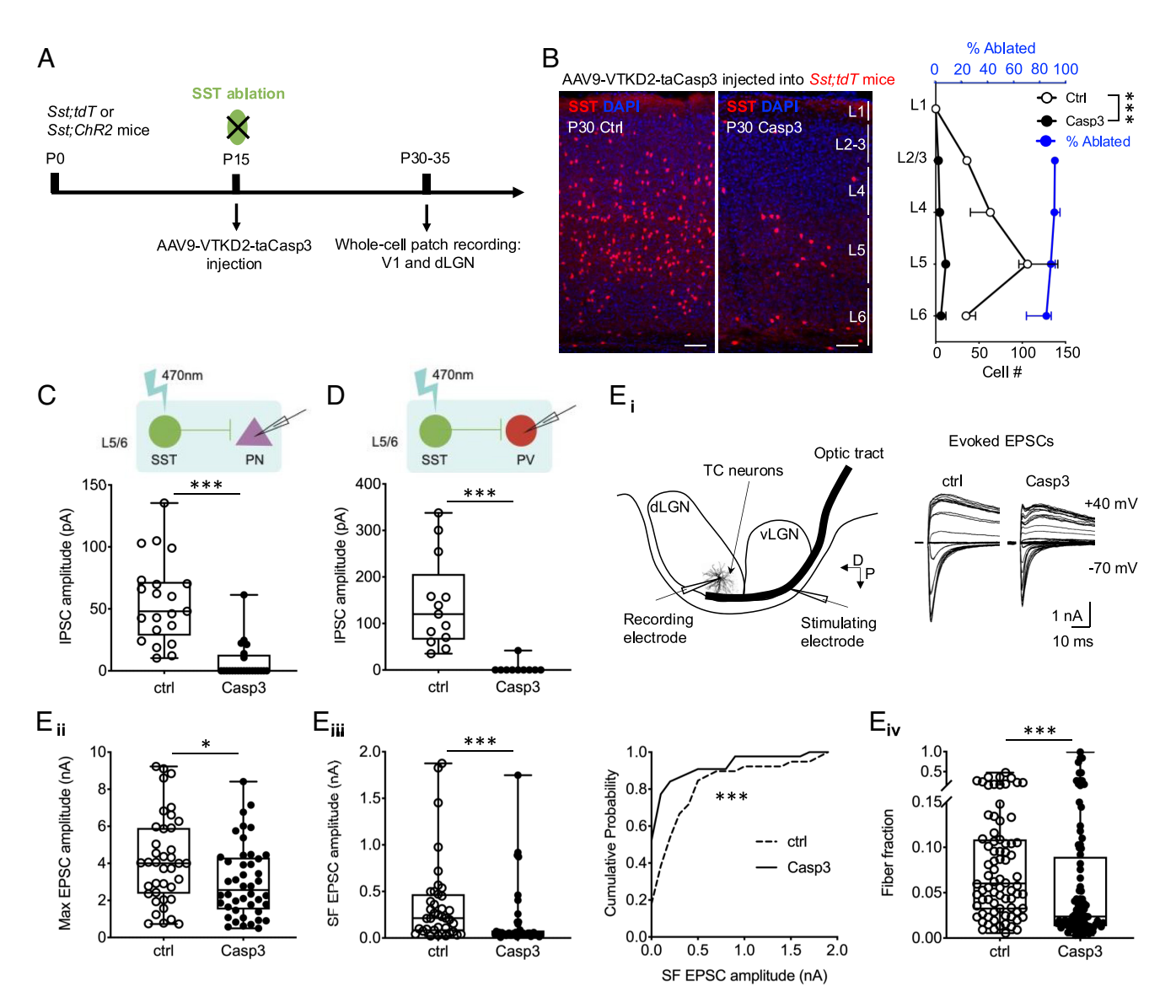


Fig. 3. Ablation of SST interneurons during development disrupts normal retinogeniculate refinement. (A) Protocol for ablating cortical SST interneurons. (B) Ablation of cortical SST interneurons across different layers in V1. (Left) Representative images of SST-tdT⁺ interneurons in the V1 from mice injected with PBS (ctrl) or Casp3-expressing virus (Casp3). (Right) Distribution of SST-tdT⁺ interneurons (black axis) and the proportion of SST interneurons ablated by Casp3 (blue axis) across V1, n = 8 mice. ****P < 0.001, two-way ANOVA. (Scale bar: 100 μ m.) (C and D) Effect of SST interneuron ablation on peak amplitude of (C) SST \rightarrow PN IPSCs and (D) SST \rightarrow PV IPSCs, both ***P < 0.001, Mann-Whitney test. (E) Measurement of retinogeniculate responses after ablation of cortical SST interneurons. (E_{ir} , Left) Schematic of recording evoked eEPSCs from TC neurons in the dLGN by electrically stimulating the bulk of optic tract. D: dorsal; P = 0.001, P = 0.

Ablation of PV Interneurons during Development Enhances Pruning of Retinogeniculate Synapses. Since SST interneurons also synapse onto PV interneurons, we investigated whether cortical PV interneurons also play a role in thalamic refinement. To directly assess their effects on retinogeniculate synapses, we used the same ablation strategy as for SST interneurons, deleting PV interneurons with *Pvalb-Cre* mice (Fig. 4 A and B). Similar to SST interneuron ablation, the number of PV interneurons started to decline by 5 d after injection, and the majority were removed across different cortical layers by 15 d after injection (SI Appendix, Fig. S4). We find that removing PV interneuron has a distinct effect on the pruning of retinogeniculate inputs onto TC neurons. The median amplitude of both maximum and SF retinogeniculate EPSCs does not differ significantly between PV-ablated mice and controls (Fig. 4 C_i and \widetilde{C}_{ii} and SI Appendix, Table S3). However, the cumulative distribution plot of SF retinogeniculate EPSC amplitudes shows a rightward shift compared to controls, with a larger proportion of retinal inputs with strengths greater than 200 pA (Fig. 4 C_{ii} , Right). Consequently, the FF significantly increases (Fig. 4 C_{iii} and SI Appendix, Table S3), indicating fewer converging retinal inputs in the absence of cortical PV interneurons. Taken together, in contrast to SST interneuron ablation, which reduces pruning, ablation of PV interneurons enhances retinogeniculate pruning beyond normal levels by P30. These results demonstrate that while PV interneurons also regulate retinogeniculate synapse refinement, their role is distinct from and opposite to that of cortical SST interneurons.

Experience-Dependent Refinement of Retinogeniculate Synapses Is Regulated by Cortical SST and PV Interneurons. Visual deprivation disrupts both the maturation of cortical SST interneuron-mediated circuits and connectivity at the

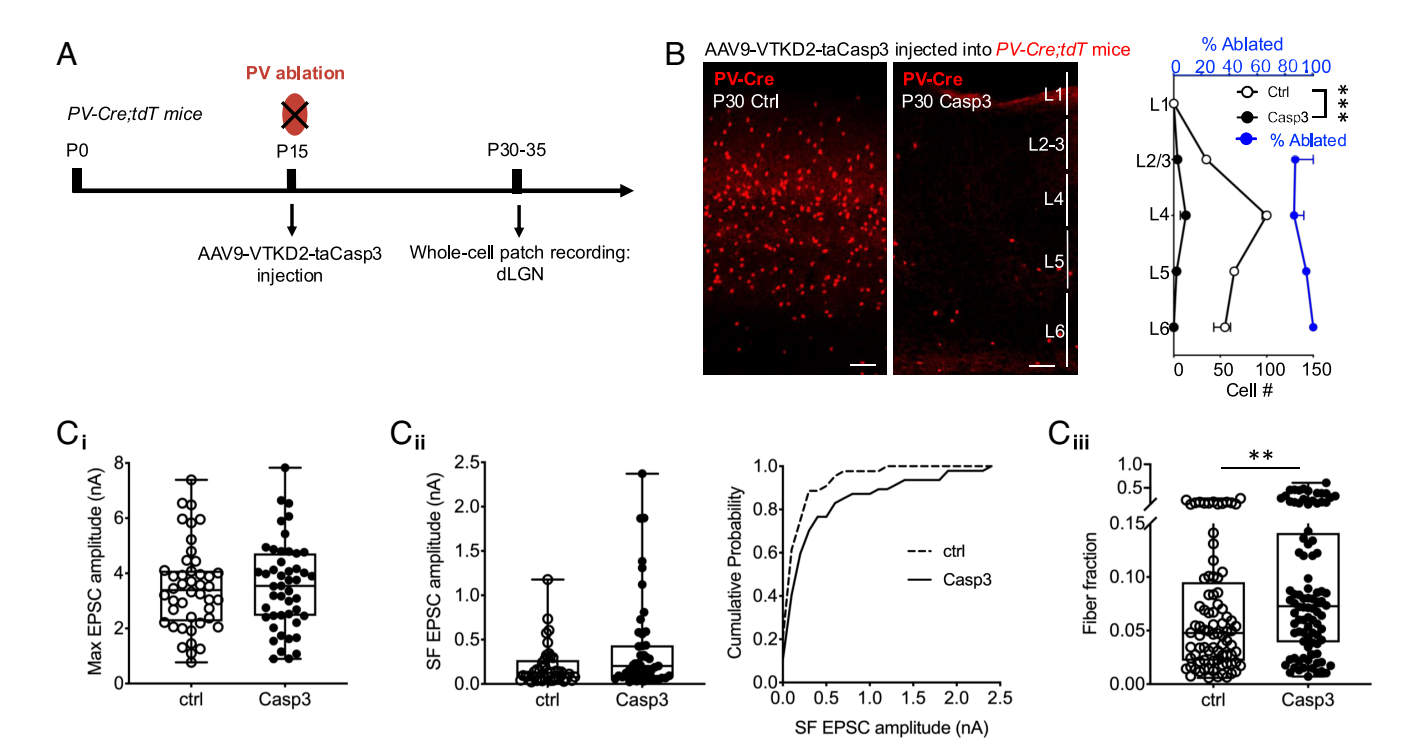


Fig. 4. Ablation of cortical PV interneurons during development accelerates retinogeniculate pruning. (A) Protocol for ablating cortical PV interneurons. (B) Ablation of PV interneurons across different layers in V1. (Left) Representative images of PV-tdT⁺ interneurons in the V1 from ctrl or Casp3-treated mice at P30. (Right) Distribution of PV-tdT⁺ interneurons across V1 (black axis) and the proportion of PV interneurons ablated by Casp3 (blue axis) (n = 3 mice). ***P < 0.001, two-way ANOVA. (Scale bar: 100 μm.) (C) Measurement of retinogeniculate responses after ablation of cortical PV interneurons. (C): Peak amplitude of the Max AMPAR EPSCs, P = 0.69, Mann–Whitney test; (C_{ij}): Peak amplitude (Left) and cumulative probability distribution (Right) of SF EPSCs. (Left) P = 0.057, Mann–Whitney test; (Right) P = 0.173, Kolmogorov–Smirnov test; (C_{ij}): Distribution of FF ratio, **P < 0.01, Mann–Whitney test.

retinogeniculate synapse (1). This raises the question of whether cortical SST interneurons regulate experience-dependent retinogeniculate plasticity through altering the activity of feedback PNs. Therefore, we selectively manipulated cortical SST interneuron activity during LDR. We expressed a Cre-dependent excitatory DREADD (hM3Dq) in cortical SST interneurons at P15 by viral injection and administered CNO through drinking water between P20 and P30 while the mice were subjected to LDR (Materials and Methods). Control mice underwent the same procedure but received vehicle viral injections instead and were divided into cohorts reared under either normal light/dark cycles or LDR (Fig. 5A). Recordings from these mice show that the median amplitudes of both maximum and SF EPSCs, as well as FF, are greater in DREADD-manipulated LDR mice compared to control LDR mice. These results show that increased SST interneuron activity prevents both the weakening of SF strength and the increase in the number of retinal inputs caused by LDR. In fact, retinogeniculate synapse refinement in LDR and DREADD-manipulated mice is not significantly different from that in normally reared control mice, suggesting that DREADD activation of cortical SST interneurons largely prevents the disrupted retinogeniculate connectivity typically observed in LDR mice (Fig. 5B and SI Appendix, Table S3). Building on previous results, our findings demonstrate that LDR impacts SST interneuron circuit maturation, whereas activation of SST interneurons counteracts the impact of LDR on retinogeniculate synapse refinement. These results suggest that developing cortical SST interneurons are functionally modulated by sensory input and, in turn, alter corticothalamic projections and their influence on thalamic synapse refinement.

Our finding that PV ablation enhances pruning raises the question of whether PV interneurons also directly participate in sensory-dependent synaptic refinement. To explore this, we ablated PV interneurons in mice subjected to LDR and measured retinogeniculate connectivity between P30-35 (Fig. 5C). Remarkably, similar to the effects observed when SST interneurons are activated, both SF strength and FF are significantly increased in PV-ablated mice compared to LDR controls, reaching levels comparable to those in normally reared control mice (Fig. 5D and SI Appendix, Table S3). These results indicate that cortical SST and PV interneurons provide complementary, bidirectional control over cortical feedback neurons, which in turn regulate retinogeniculate connectivity.

SST Interneurons Modulate the Maturation of PV Interneuron Firing Properties. Up to this point, we have examined the overall effects of SST and PV interneurons by manipulating them separately, demonstrating their opposing effects on the refinement of retinogeniculate synapses. Yet, whether there is an interaction between these two types of interneurons is not clear. Given that SST interneurons mature earlier and form increasingly stronger synapses onto PV interneurons during development (Fig. 1 C), this interaction may play a role in balancing their opposing influences on top-down regulation of thalamic synapse refinement. Our results showed that the developmental strengthening of SST \rightarrow PV synapses does not appear to be influenced by sensory experience (Fig. 2B). To investigate further, we tested whether SST interneurons impact other aspects of PV interneuron maturation in a sensory experience-dependent manner. Given the late onset of PV expression, we first examined whether PV expression correlates with the electrophysiological maturation of PV interneurons. By recording from PV-tdT⁺ neurons in L6 of *Pvalb-tdT* mice, we observed heterogeneity in their firing patterns in response to current injections between P15 and P30 (Materials and Methods). We identified three distinct firing patterns: single-spiking, slow-spiking (with a maximum firing rate below 40 spikes/s,

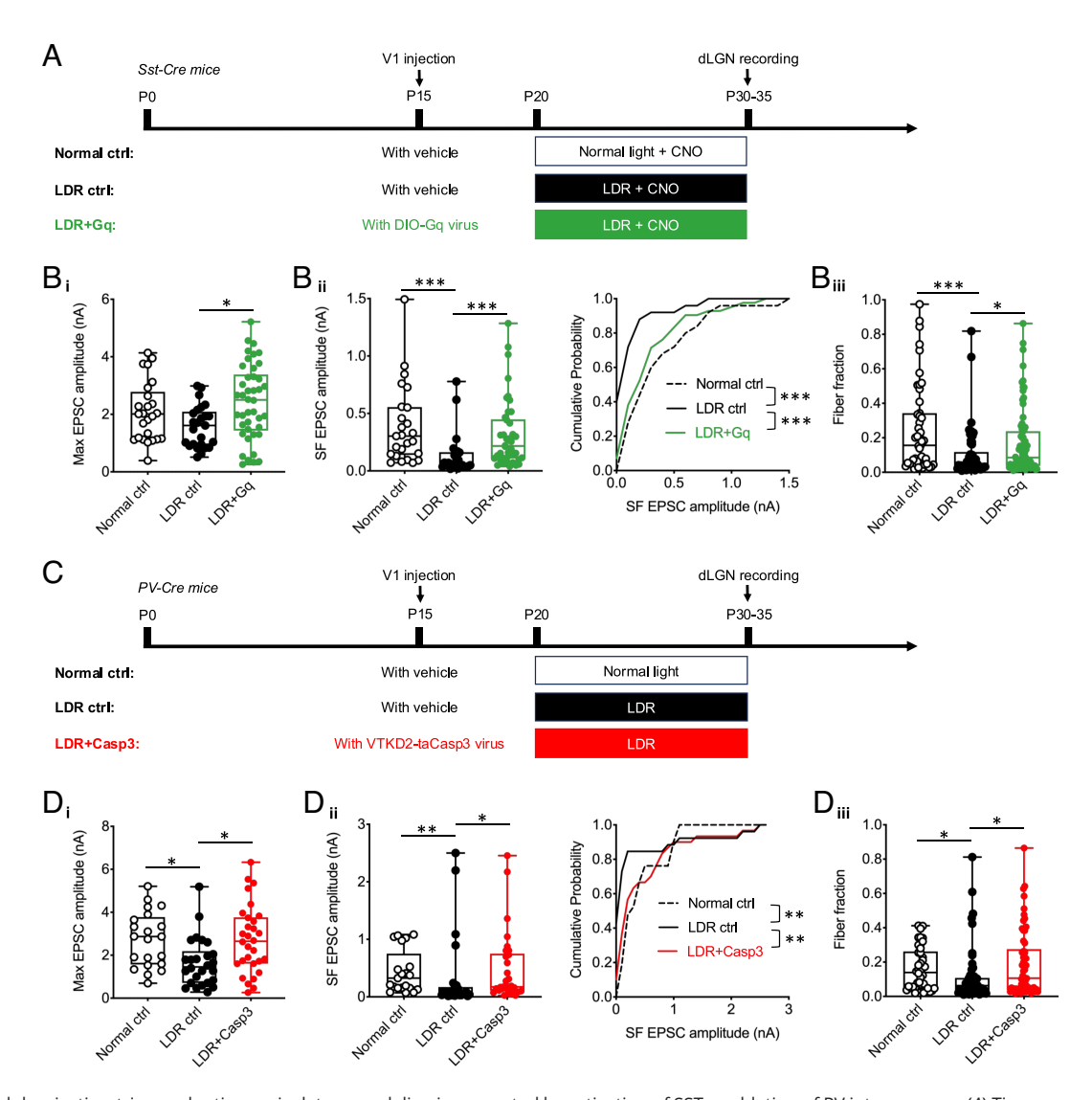


Fig. 5. Visual deprivation-triggered retinogeniculate remodeling is prevented by activation of SST or ablation of PV interneurons. (*A*) Time course for activation of SST interneurons and visual deprivation. (*B*) Activation of SST interneurons during P20-30 prevented the alteration of retinothalamic connections caused by LDR. (*B*): Peak amplitude of the Max AMPAR EPSCs, *P < 0.05, Kruskal-Wallis test. (P_0): Peak amplitude (Left) and cumulative probability distribution (Right) of SF EPSCs, ***P < 0.001, Kruskal-Wallis test and Kolmogorov-Smirnov test, respectively; (P_0): Distribution of FF ratio, *P < 0.05, ***P < 0.01, Kruskal-Wallis test. (*C*) Time course for ablation of PV interneurons and visual deprivation. (*D*) Ablation of PV interneurons during P20-30 occludes the remodeling of thalamic refinement triggered by LDR. (P_0): Peak amplitude of the Max AMPAR EPSCs, *P < 0.05, Kruskal-Wallis test; (P_0): Peak amplitude (P_0): Distribution of FF ratio, *P < 0.05, Kruskal-Wallis test.

SI Appendix, Fig. S5A), and fast-spiking (with a maximum firing rate above 50 spikes/s, SI Appendix, Fig. S5B). At P15, only 16% of tdT+ cells are fast-spiking, while the majority are single- or slow-spiking (Fig. 6A). The fraction of fast-spiking tdT+ cells increases to 65% at P20, and reaches 100% at P30 (Fig. 6A), accompanied by a developmental reduction of the action potential half-width, rise, and decay times (SI Appendix, Fig. S5 *C–E*). The shift in the firing pattern of PV interneurons may indicate developmental maturation over time. Alternatively, it could represent a transition between different PV categories. To distinguish between these two scenarios, we analyzed Pvalb expression in different PV interneuron subtypes over development (38, 39). Consistent with genetic labeling of PV in Pvalb-tdT mice, there is a steady increase in the expression of *Pvalb* from P10 to P28 in all PV interneuron subtypes (SI Appendix, Fig. S6). These findings argue against the possibility of developmental shift in PV interneuron subtypes in L6 or across the whole cortex. Instead, PV interneurons gradually acquire their mature firing properties

over an extended developmental period before P30. In contrast, SST interneurons assume their mature spiking properties much earlier, before P22-24 (40).

To explore how the maturation of PV interneuron electrophysiological properties is linked to developmental changes in the SST→PV synapse, we grouped the SST→PV synaptic responses into two categories according to PV firing properties: single to slow-spiking (immature) vs. fast-spiking (mature). We found that the median amplitude of SST-evoked IPSCs onto single to slow-spiking PV cells significantly increases between P15 and P20 (Fig. 6B and SI Appendix, Table S2), consistent with stronger SST synaptic charge transfer onto immature PV interneurons at P20 (SI Appendix, Fig. S5F). In contrast, the strength of SST input onto fast-spiking PV interneurons is weaker and does not change significantly between P15 and P30 (Fig. 6B and SI Appendix, Table S2). These results are consistent with a transient strengthening of SST→immature PV synapses during development, followed by a net reduction in the average

strength of all SST→PV inputs (both immature and mature PV interneurons) as PV interneurons become fast-spiking. The strong inhibition of immature PV interneurons might serve to promote the maturation of PV interneurons, or to prevent the "brake" on pruning from occurring prematurely.

To investigate how SST interneurons influence the maturation of PV firing properties, we repeated the ablation of SST interneurons as before. While the number of PV interneurons remains unchanged after SST interneuron ablation (*SI Appendix*, Fig. S3*B*), 23.1% of these PV interneurons exhibit single to slow-spiking patterns at P30 (Fig. 6C). This finding underscores the significant role of SST interneurons in the final maturation of PV interneuron electrophysiological properties. Intriguingly, a similar fraction (~17%) of PV cells exhibit single to slow-spiking pattern at P30 after LDR (Fig. 6 D and E). These results suggest that SST interneurons promote the electrophysiological maturation of PV interneurons in response to sensory input. By doing so, they help activate PV interneurons, which then act as a counterbalancing force alongside SST interneurons to fine-tune the activity of L6 PNs. These changes in activity, in turn, regulate retinogeniculate synapse pruning.

Discussion

There is growing evidence supporting the idea that experiencedependent plasticity engages bidirectional circuits between the thalamus and primary visual cortex (V1) (5, 41, 42). Circuit refinement within these two visual regions does not occur independently and sequentially but rather entails interactions between feedforward and feedback projections (43-49). In the present study, we identify key components of vision-dependent cortical feedback circuits responsible for refinement of feedforward retinogeniculate connectivity during late development. Here, we offer a working model based on our results which may serve as a foundation for refining our understanding of corticothalamic interactions during development in future studies.

A Reciprocal Antagonistic Mechanism of Cortical Inhibition Contributes to Top-Down Regulation of Retinogeniculate Refinement. The most parsimonious interpretation of our results is that SST interneurons in V1 contribute to driving the strengthening and pruning of the retinogeniculate synapse as both cortical and thalamic circuits remodel to incorporate visual experience into their connectivity. In contrast, the continued maturation of cortical PV circuits plays a role in limiting retinogeniculate pruning, by slowing down or "braking" the consolidation of thalamic circuits during the sensitive period so that experience-dependent changes can still be made (50–53). The balance between the two opposing cortical circuits shifts over the course of the sensitive period such that the influence of PV circuits increases with age and retinogeniculate connectivity stabilizes by the end of the period.

We propose that this shift in balance is coordinated by SST interneuron-mediated maturation of PV neuron spiking. Supporting this model, our findings reveal that SST interneurons develop earlier than PV interneurons. As SST interneurons mature, they shape the development of the infragranular circuits within V1 and promote retinogeniculate refinement by increasing inhibitory influence on the activity of L6 PN neurons. This model aligns with findings in the supragranular circuits of V1 (L2/3) where SST interneurons exert a gradually stronger effect on the response gain of PNs over a similar developmental period (54).

This model is also consistent with our findings that with SST interneuron ablation (and presumably also LDR), there is reduced inhibition onto L6 PNs, shifting the balance of forward circuit maturation and PV circuit braking toward the latter. Increased braking thus slows refinement, leading to a greater number of convergent retinal inputs that are weaker. Conversely, ablation of PV interneurons leads to a shift of the reciprocal balance toward accelerated refinement of the retinogeniculate synapse (Fig. 7). Taken together, our results support a critical role for cortical SST and PV interneurons in initiating top-down influence of thalamic refinement.

Interactions between SST and PV Interneuron Circuits over **Development.** Our results are consistent with a growing body of evidence demonstrating that the maturation of the cerebral cortex is regulated by the interplay of SST and PV interneurons. Here, our study also shows how the relationship between SST and PV circuits impacts thalamic development. The fact that ablation of PV interneurons displays an opposite outcome in retinogeniculate pruning to that when SST interneurons are ablated rules out a simple feedforward model where PV interneurons act solely as a downstream mediator of SST interneurons. Instead, the functional output of the circuitry between SST and PV interneurons likely involves network interactions in the cortex. In particular, the results from ablation of PV interneurons in LDR mice are illuminating. If the influence on retinogeniculate refinement was dependent on the absolute level of activity of SST vs. PV interneurons, it would be hard to explain how reduction of both SST and PV interneuron drive leads to normal retinogeniculate connectivity. Instead, we suggest that it is the balance of SST vs. PV interneuron circuit drive that is important (Fig. 7B). Yet SST and PV interneuron circuits are not fully independent, as we find that LDR or ablation of SST interneurons at around P20 prevents the final maturation of PV interneuron excitability. Therefore, full cortical influence on retinogeniculate refinement depends on both independent SST and PV interneuron circuits as well as complex interactions between these circuits that have been recently demonstrated (23, 55).

Experience-Dependent Plasticity of the Corticothalamic Circuit.

Our finding that the sensitivity of SST circuits to visual experience -mirrors that of the retinogeniculate synapse highlights a distinct relationship between these specific cortical and thalamic circuits. These findings are different from previous reports of experiencedependent refinement of other visual cortical circuits. Complete deprivation of visual experience from birth (referred to as chronic dark rearing, CDR) is known to prevent the maturation of visual acuity and the development of PV interneuron circuits (56-59). Studies have demonstrated that prolonged deprivation decreases GAD65- and GAD67-immunopositive perisomatic puncta on PNs and PV expression (60-63). In contrast, neither the density of SST⁺ interneurons nor the expression of SST is changed in the cortex by CDR (57, 60). Dark rearing from P20 (LDR) is a very different manipulation from CDR as much of the inhibitory circuitry has already developed by this time. Moreover, we find that SST→PN synaptic transmission is not sensitive to CDR (SI Appendix, Fig. S2E). Notably, our previous studies showed that CDR did not elicit the same retinogeniculate plasticity as LDR—instead retinogeniculate refinement appeared normal (1, 2). Taken together, our results demonstrate that different cortical inhibitory circuits exhibit sensitivity to visual experience during distinct windows of development.

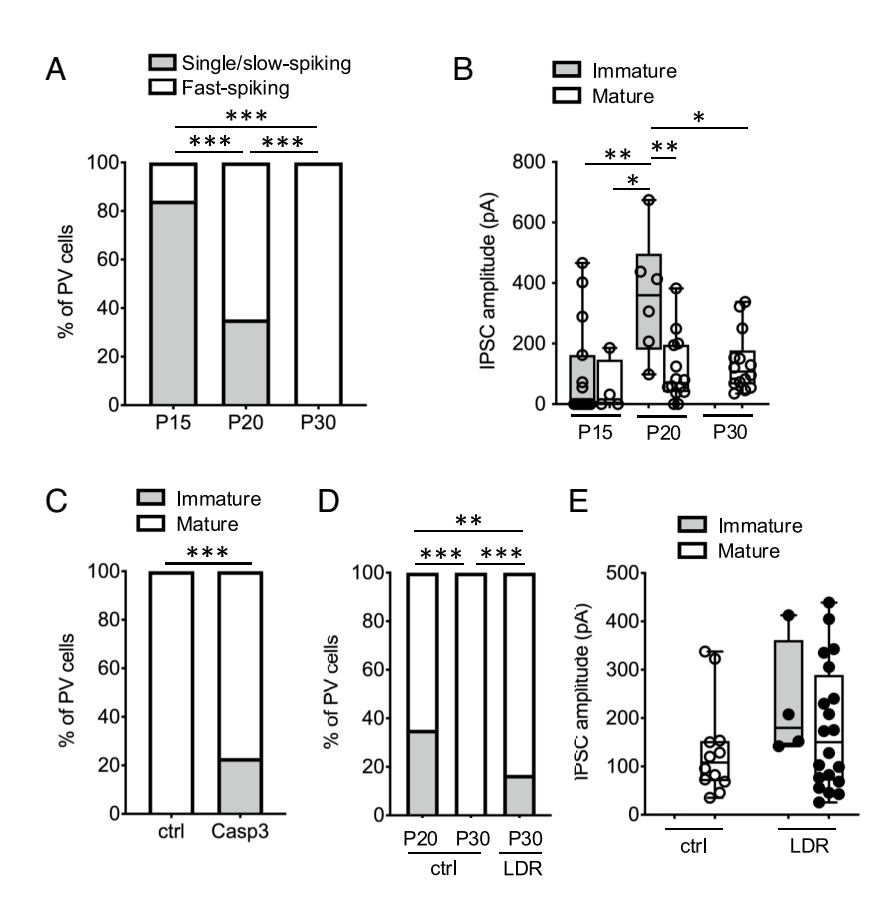


Fig. 6. SST interneurons modulate the maturation of PV interneuron firing properties. (*A*) Fractional distribution of single/slow-spiking vs. fast-spiking PV interneurons during development. ***P < 0.001, chi-square test. (*B*) Amplitude of SST \rightarrow PV IPSCs in immature (single/slow-, gray bars) vs mature (fast-, white bars) PV interneurons during development. *P < 0.05, **P < 0.01, two-way ANOVA, Sidak's multiple comparisons test. (*C*) Fractional distribution of immature vs mature PV interneurons after ablation of SST interneurons. ***P < 0.001, chi-square test. (*D*) Fractional distribution of immature vs. mature PV interneurons after LDR. **P < 0.01, ***P < 0.001, fisher's exact test. (*E*) Median amplitude of SST \rightarrow PV IPSCs sorted by maturation state of PV cells after LDR.

Summary

While our working model of synaptic refinement in the geniculate is consistent with cortical SST interneurons accelerating and PV interneurons attenuating synaptic refinement, intracortical circuits are complex. Although our previous evidence demonstrates that retinogeniculate remodeling can be modulated by alterations in corticothalamic feedback (5), it remains unclear how this pathway is controlled by interneuron dynamics. Work in both the somatosensory (16, 19, 23, 64, 65) and the visual system (17, 18, 20) indicates that the transition from synchronous to decorrelated activity in the cerebral cortex involves a developmental shift in the role of early SST to PV activity (14, 21-24). While the events studied here occur subsequent to this timepoint, it is likely that further maturation of interactions between cortical SST and PV interneurons results in increasingly sparse and complex higherorder cortical activity, which we here suggest sequentially alters top-down signaling to impact retinogeniculate development. Nonetheless, the specifics by which the actions of interneurons may involve additional cortical lamina and further recurrent circuits will require further investigation. Future studies simultaneously recording the activity of populations of identified neuronal types across cortical lamina will help further advance our understanding of these developmental corticothalamic interactions (54).

Materials and Methods

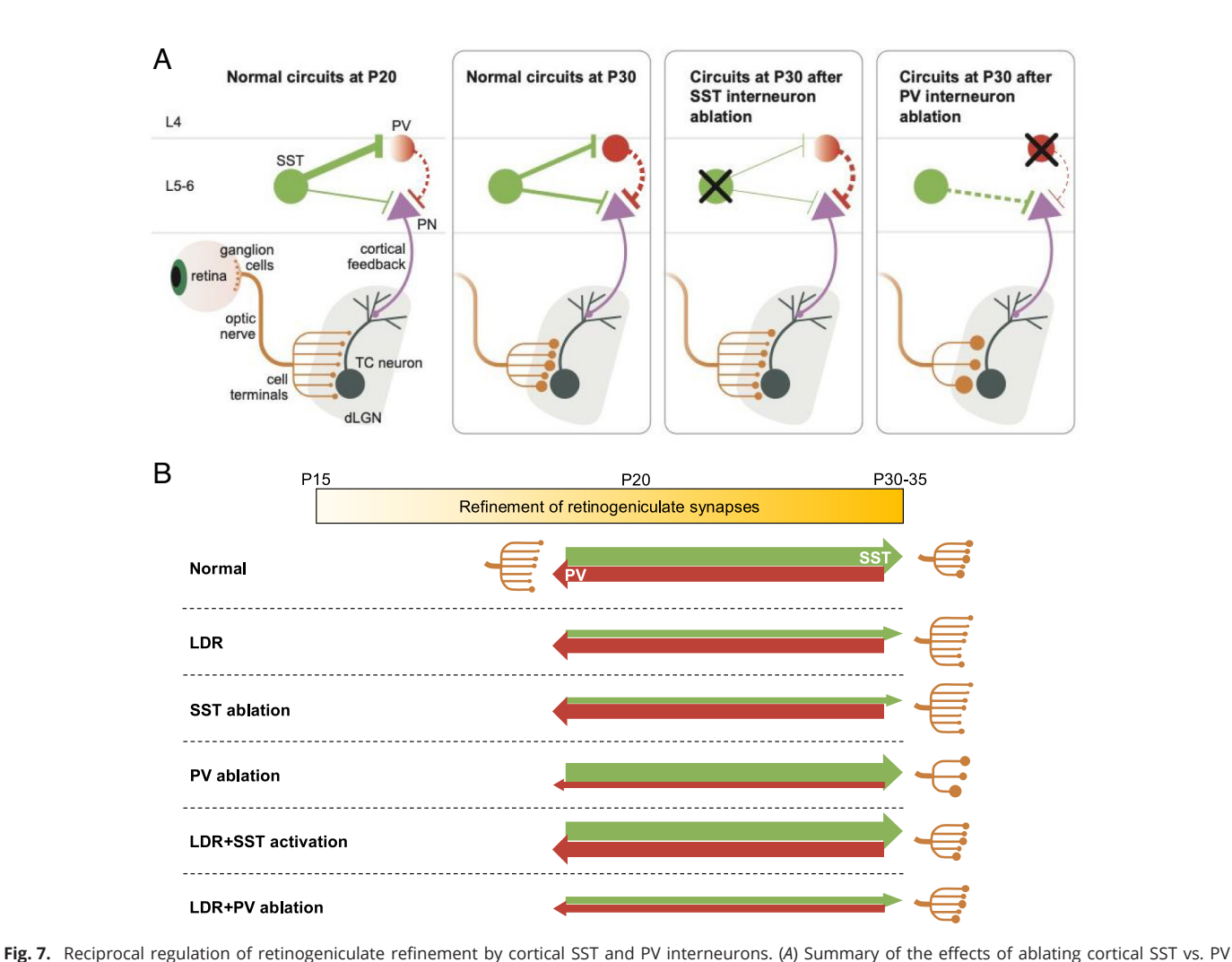
Animals. All animal procedures were in compliance with the NIH Guide for the Care and Use of Laboratory Animals and approved by the Institutional Animal and Care and Use Committee (IACUC) at Boston Children's Hospital. To label and drive SST interneurons in the V1, Sst-IRES-Cre (Sst-Cre) transgenic mice (JAX 013044) were crossed with fluorescently tagged Cre-dependent tdTomato expressing mice (Ai14, JAX 007908) (66), or ChR2-EYFP expressing mice (Ai32, JAX 012569) (67). We refer to the resulting crosses as "Sst;tdT" and "Sst;ChR2",

respectively. *Sst;ChR2* mice were also crossed with *Pvalb-tdT* transgenic mice (JAX 027395) to yield *Pvalb;Sst;ChR2* progenies for examining SST inhibitory transmission onto PV interneurons in V1. *Pvalb-Cre* mice were obtained from Dr. Clifford Woolf's lab to ablate PV interneurons specifically (JAX 017320) (68). They were crossed with *Ai14* mice to yield *Pvalb-Cre;tdT* progenies to detect the developmental distribution of PV-Cre⁺ interneurons in the cortex. Mice aged P10-P60 of either sex were used. For chronic CNO treatment, mice had ad libitum access to CNO-treated water (0.25 mg/mL) instead of regular drinking water.

Visual Deprivation. For LDR, mice were subjected to dark rearing during P20-(~30). At desired ages, they were killed in the dark for slice preparation. For CDR, the pups were placed in dark boxes right after birth together with their mother and killed in the dark without exposure to normal light.

Tissue Preparation and Immunohistochemistry. Mice were anesthetized with 50 mg/kg pentobarbital and transcardially perfused with 0.1 M phosphate-buffered saline (PBS) immediately followed by 4% w/v paraformaldehyde (PFA) in PBS. Brains were postfixed overnight in 4% PFA at 4 °C and rinsed in PBS. Brain slices containing V1 were coronally sectioned through Leica VT1000 vibratome with thickness of 60 μm .

For immunostaining, brain slices containing V1 were blocked in PBS containing 5% normal goat serum (NGS) and 0.1% Triton X-100 at room temperature for 1 h. Then, primary antibodies were applied in PBS containing 0.1% Triton and 2% NGS: chicken anti-green fluorescent protein (GFP, 1:1,000; ab13970, Abcam), and/or rabbit anti-RFP (1:1,000; 600-401-379, Rockland), and/or rabbit anti-PV (1:1,000; PV27, SWant) at 4 °C overnight. After rinsing with 0.1% Triton/PBS in the next day, the slices were incubated with secondary antibodies at room temperature for 2 h: goat anti-chicken antibody conjugated to Alexa Fluor 488 (1:1,000; A11039, Invitrogen), and/or goat anti-rabbit antibody conjugated to Alexa Fluor 488 (1:1,000; ab150077, Abcam), or 555 (1:1,000; A32732, Invitrogen). Slices were then incubated with DAPI for nuclear detection, mounted, and cover-slipped with Vectashield (VectorLabs H-1000). For the quantification of V1 corticothalamic neurons, a combination of primary antibodies: rabbit anti-GABA (1:1,000; A2052, Sigma), mouse anti-Tle4 (1:100; sc-365406, Santa Cruz), and chicken anti-NeuN (1:1,000; ABN91, Millipore Sigma); and secondary antibodies: goat anti-rabbit Alexa 647 (1:1,000; A21245, Invitrogen), goat anti-mouse Alexa



interneurons on the refinement of retinogeniculate synapses in the dLGN. The thickness of the green/red lines in the V1 indicates the relative strength of inhibition from SST/PV interneurons. Dashed lines represent speculated changes in the strength of connectivity. In normal development from P20 to P30, when retinal inputs undergo experience-dependent strengthening and pruning, cortical SST interneurons mediate the maturation of infragranular inhibitory circuits. When SST interneurons are ablated between P20 and 30, PV interneurons take over the role as being the main inhibitor of PNs, resulting in retinogeniculate synapses being much less refined in the dLGN. On the contrary, loss of PV interneurons between P20-30 leads to an acceleration in the pruning of retinal inputs compared to normal circuits in the thalamus. (B) Schematic for the opposing forces between cortical SST driving forward development (green arrows) and PV interneurons braking refinement (red arrows). The thickness of the arrow bars indicates the relative strength from driving vs. braking refinement. During normal development, SST and PV interneurons form a balance in the driving vs. braking system to determine the timing of strengthening and pruning of retinal inputs over age. After LDR or ablation of SST interneurons, the balance of forward vs. braking refinement shifts, leading to less refined thalamic circuits. On the contrary, with PV interneuron ablation, the brakes are removed, allowing thalamic circuits to develop more rapidly. Enhanced SST interneuron activity overrides LDR effects, while PV ablation during LDR establishes a new balance between the opposing drives of SST and PV interneuron.

555 (1:1,000; A32727, Invitrogen), and goat anti-chicken Alexa 488 (1:1,000; A11039, Invitrogen) were used for the staining of slices containing V1.

Single Molecule Fluorescent In Situ Hybridization (smFISH) Histochemistry. For smFISH combined with immunohistochemistry, mice were perfused and brains were fixed overnight in 4% PFA in 1× PBS followed by cryoprotection in 30% sucrose in 1 \times PBS. Then, 16 to 20 μm thick brain sections were obtained using a Leica cryostat. The sectioned brain slices were directly mounted on glass slides (Fisherbrand Superfrost Plus) and preserved in −80 °C freezer.

For RNAscope experiments, samples were processed according to the ACDBio Multiplex Fluorescent v2 Kit protocol (ACDBio #323100) for fixed frozen tissue. Briefly, tissue was pretreated with a series of dehydration, H₂O₂, antigen retrieval, and protease III steps before incubation with the probe for 2 h at 40 °C. Note here protease III incubation was performed at room temperature to better preserve the protein for immunostaining. The probes used for labeling included 1) RNAscope Probe-Mm-Pvalb (Cat#421931-C3, ACDBio); and 2) RNAscope Probe-Mm-Gad1 (Cat#400951, ACDBio). Three amplification steps were carried out prior to developing the signal with Opal™ or TSA® Dyes (Akoya Biosciences). Immunostaining following RNAscope experiment was performed according to Technical Note 323100-TNS from ACDBio. Samples were counterstained with

DAPI and mounted using Prolong Gold antifade mounting medium (Molecular Probes #P369300).

 $\textbf{Imaging and Image Analysis.} \ To \ measure \ the \ expression \ of \ SST-tdT^+, PV-tdT^+,$ PV⁺, or PV-Cre⁺ neurons over development or over time after injection of viruses, images of the V1 (one coronal full view containing both monocular and binocular regions from each animal) from at least three mice were acquired with Zeiss LSM 700 (Zeiss, Olympus) using a 10× objective. Scans were performed to obtain 9 to 11 optical Z sections of 6 µm each. Quantification was performed manually using ImageJ. The images were stacked over the whole slice with thickness of ~60 µm. The number of tdT⁺ or PV⁺ neurons were then counted manually from each layer in the V1, including L1, L2/3, L4, L5, and L6. For the identification and measurement of single molecule signals of Pval and Gad1 following RNAscope experiment, or the assessment of overlap among molecules of Tle4, NeuN, and GABA, V1 images were acquired through Zeiss LSM 700 using 40× and 63× objectives with built-in functions of Z-stack. Consecutive images (0.9 µm thick each) were collected for analysis. Maximum projection and cell counting were conducted through ImageJ. In the RNAscope images, a cluster of single molecules was identified as belonging to one cell when they colocalized with DAPI and formed a clear cell morphology.

Viral Injections. Mice were anesthetized via 2% of isoflurane (Baxter, IL) and fixed onto the stereotactic platform. Viruses expressing Casp3 were microinjected using NanojectIII (Drummond, PA) at 1 nL/s to three sites of the right hemisphere of V1 to cover both monocular and binocular zones. The following coordinates were used: P15: from Lambda AP+0.7, ML+2.4, DV-0.55; AP+1.4, ML+2.7, DV-0.55; AP+0.7, ML+2.9, DV-0.55; P30: from Lambda AP+0.8, ML+2.35, DV-0.55; AP+1.5, ML+2.35, DV-0.55; AP+0.8, ML+2.95, DV-0.55 (in mm). Virus AAV9-VTKD2-taCasp3-TEVp (shared by Gord Fishell's lab) was used for ablation of SST or PV interneurons, and AAV2/9-hSyn-DIO-hM3D(Gq)-mCherry (Addgene #44361) for activation of SST interneurons. The mice were perfused for immunostaining or killed for patch recording at required ages. Control (ctrl) mice and those injected with Casp3-expressing virus were housed together and randomly assigned to the experimenter for patch recording blind of condition.

Electrophysiology. Brain slices for in vitro recordings were prepared as previously described (69, 70). Briefly, mice were anesthetized using isoflurane and decapitated into oxygenated (95% O₂; 5% CO₂) ice-cold cutting solution (in mM): 130 K-gluconate, 15 KCl, 0.05 ethylene glycol-bis(β-aminoethyl ether)-N,N,N',N'tetraacetic acid (EGTA), 20 4-(2-hydroxyethyl)-1-piperazineethanesulfonic acid (HEPES), and 25 glucose (pH 7.4 adjusted with KOH, 310 to 315 mOsm) (71). The brain was then removed quickly and immersed in the ice-cold cutting solution for 60 s. For V1 recording, coronal slices containing V1 were sectioned and collected. For dLGN recording, parasagittal sectioning was conducted to obtain slices maintaining continuity of optic tracts (OT) as previously described (72). The brain was cut with a steel razor blade, then sectioned into 250 μm -thick slices in the oxygenated ice-cold cutting solution using a sapphire blade (Delaware Diamond Knives, Wilmington, DE) on a vibratome (VT1200S; Leica, Deerfield, IL). The slices collected were allowed to recover at 30 °C for 15 to 20 min in oxygenated saline solution (in mM): 125 NaCl, 26 NaHCO₃, 1.25 NaH₂PO₄, 2.5 KCl, 1.0 MgCl₂, 2.0 CaCl₂, and 25 glucose (pH 7.4, 310 to 315 mOsm).

For cortical recordings, PV interneurons or PNs in V1 L6 were visualized through a monitor with projection from the camera of a microscope equipped with Differential Interference Contrast (DIC) system (Prime BSI, Teledyne Photometrics). While PV interneurons were genetically labeled in Pvalb-tdT mice, PNs were identified based on their distinct pyramid-like shape and relatively larger size compared to interneurons. L6 was identified as no more than 200 μ m away from the white matter. Glass pipettes (Drummond Scientific) were pulled on Sutter P-97 Flaming/Brown micropipette puller (Sutter Instruments) and filled with internal solution containing (in mM): 150 K-gluconate, 8 KCl, 10 EGTA, 10 HEPES (pH 7.3, 290 to 300 mOsm) to optimize the pipette resistance to be 3.5 to 4.0 MOhm. Patch recordings were performed using a MultiClamp 700B (Axon Instruments, Foster City, CA) and an ITC-18 interface (Instrutech) with sampling rate of 2 kHz and filtering frequency of 5 kHz. IPSCs were obtained by holding the membrane potential at 0 or 30 mV and applying a single pulse (0.2 ms) of full-field illumination of blue light (470 nm) through the $60 \times$ objective (Olympus LUMplanFL N $60 \times /1.00$ W), thus to confine the illumination to an area with a radius of \sim 220 μ m within the infragranular layers without surpassing L4. The blue light was supplied by a CoolLED pE unit, lasting for 0.2 ms at highest power (100%, 83 mW/mm²) to obtain maximal current. Intertrial intervals were kept at 1 min. Access resistance was monitored throughout the experiment and evaluated in offline analysis. Experiments with access resistance changing over 20% were removed from analysis. Spiking of SST interneurons and intrinsic cellular properties of PNs and PV interneurons were measured in current clamp mode. I-V curves were obtained by recording firing rates when using current injection from 0 to 600 pA in steps of 50 pA. The activation of SST interneurons was verified by continuous blue light illumination for 1 s, or single pulse (0.2 ms) photostimulation in current clamp mode.

To measure retinogeniculate refinement, TC neurons located in the ventral posterior region of the dLGN were recorded as previously described (1, 73). Glass pipettes were filled with internal solution containing (in mM): 35 CsF, 100 CsCl, 10 EGTA, 10 HEPES, and L-type calcium channel antagonist 0.1 methoxyverapamil (pH 7.3, 290 to 300 mOsm) to optimize the pipette resistance to be 1.5 to 2.0 MOhm. Both AMPAR and NMDAR currents were obtained by holding the membrane potential of recorded cells at -70 and +40 mV, respectively. To isolate excitatory synaptic currents, cells were recorded at room temperature in oxygenated saline solution containing 20 μ M of bicuculline (GABA $_{\rm R}$ R antagonist), 2 μ M of CGP55845 (GABA $_{\rm R}$ R blocker), 10 μ M of DPCPX (antagonist of A1 adenosine receptors), and 50 μ M of LY341495 (blocker of presynaptic mGluRs) (74–78). To obtain maximal electrical stimulated EPSCs, a

pair of electrodes were filled with saline solution, and lowered onto the slices. One of the electrodes was inserted into the OT to electrically stimulate the retinogeniculate inputs. The other electrode was immersed in the bath just above the brain slice surface, serving as the ground. Electrical stimuli were supplied by a stimulus isolator (WPI A365) delivering a 0.2 ms pulse between 0 to 99 mA. Maximal currents were defined as the largest response that does not increase with higher stimulating intensity (up to 99 mA). SF strength was defined as the first consistent response observed after an increase in stimulation intensity by 0.25 µA. FF was calculated as SF strength over maximal current, as an estimate of the contribution of a single input to the total retinal drive. AMPAR currents were included in the analysis of maximal currents and SF input, while both AMPAR and NMDAR currents were used for the calculation of FF. Given the fact that there is a great deal of variance in the strength of retinogeniculate inputs, even at the mature synapses, the FF values are meant to be used to compare relative changes in retinogeniculate convergence as we have previously described (1, 5, 69, 70). For each experimental condition, we assigned the mice from the same litter into control and experimental cohorts. Comparison of recorded values from controls from different experiments showed no significant difference in the median values or cumulative distributions (SI Appendix, Table S3).

Source and Processing of snRNA-seq Datasets. The P8, P14, P17, P21, P28 single-nucleus RNA sequencing (snRNA-seq) datasets of V1 were downloaded (https://singlecell.broadinstitute.org/single_cell/study/SCP1664/vision-dependent-specification-of-cell-types-and-function-in-the-developing-cortex#study-summary) and interneuron subtypes were classified from these datasets (39). Detailed acquisition and analysis procedures of the snRNA-seq dataset of P10 interneurons from V1 will be included in a subsequent publication (79). In brief, tissue from the visual cortex was dissected from Dlx5/6-Cre (JAX #008199)::CAG-Sun1/sfGFP (JAX #030952) mice. Nuclei were isolated as described before (80) and subsequently sorted on Sony SH800S cell sorter for GFP+ nuclei. snRNA-seq libraries were prepared using Chromium single cell 3' library and gel beads kit (10×genomics, PN-1000075). CellRanger (v7.0.0, 10× Genomics) was used with default parameters to map snRNA-seq data to the mouse reference genome (mm10) provided by 10× Genomics. Datasets from different ages were integrated using the pipeline (https://github.com/genecell/PIASO).

Data Analysis and Statistics. Electrophysiological data acquisition and offline analysis were performed using custom software in IgorPro (Wave-Metrics, Portland, OR). EPSC and IPSC amplitudes were obtained from average traces of 3 to 5 trials. Data calculation and statistical analysis were conducted using Prism (GraphPad Software, Inc.) and MATLAB_R2019b (Mathworks). All datasets were evaluated for normality using the Kolmogorov-Smirnov test. For nonparametric distributions, the Mann-Whitney or Kruskal-Wallis test was used for comparisons between two or among multiple groups. For normally distributed datasets, the Student's *t* test or one-way ANOVA was used. For comparison of time series repeated measurements, two-way ANOVA test was used. The F test was used for comparison of variances between two groups. All data were presented as medians (interquartiles). The box and whisker graphs indicate the median (line within box), 25 to 75% quartile range (box), and minimum and maximum range (whiskers). For all figures, *P < 0.05; **P < 0.01; ***P < 0.001.

Data, Materials, and Software Availability. All study data are included in the article and/or *SI Appendix*.

ACKNOWLEDGMENTS. We thank Drs. April Levine, Brielle Ferguson, John Assad, and all other members of the Chen lab for helpful discussions about the project and manuscript. We thank Jianlin Wang, Israel Robinson, and Iris Wu for blinding the experimenter, Julia Kuhl for designing the schematics in the paper, and Shuhan Huang from Dr. G.F.'s lab for providing the AAV9-VTKD2-taCasp3 virus. Support was provided by the NIH RO1EY013613 and Tan-Yang Center for Autism Research Grant to C.C., William Randolph Hearst Fund 520.45318.7900.600377.730002.0 000.65852 to Q.J., and NIH 5R01NS081297 to G.F. We thank the Intellectual and Developmental Disabilities Research Center (IDDRC) Cellular Imaging Core, funded in part by S100D016453 for access to their shared confocal microscopes, as well as P50HD105351 for the Cellular Imaging and Administrative cores.

Author affiliations: ^aDepartment of Neurology, F.M. Kirby Neurobiology Center, Boston Children's Hospital, Harvard Medical School, Boston, MA 02115; ^bDepartment of Neurobiology, Blavatnik Institute, Harvard Medical School, Boston, MA 02115; and ^cStanley Center for Psychiatric Research, Broad Institute, Cambridge, MA 02142

- B. M. Hooks, C. Chen, Distinct roles for spontaneous and visual activity in remodeling of the retinogeniculate synapse. Neuron 52, 281-291 (2006).
- B. M. Hooks, C. Chen, Vision triggers an experience-dependent sensitive period at the retinogeniculate synapse. J. Neurosci. 28, 4807-4817 (2008).
- L. Liang, C. Chen, Organization, function, and development of the mouse retinogeniculate synapse. Ann. Rev. Vision Sci. 6, 261-285 (2020).
- C. Chen, "Mechanisms underlying the refinement of the retinogeniculate synapse" in The Cerebral Cortex and Thalamus, C. Chen, W. M. Usrey, S. M. Sherman, Eds. (Oxford University Press, 2023), 10.1093/med/9780197676158.003.0049.
- A. D. Thompson, N. Picard, L. Min, M. Fagiolini, C. Chen, Cortical feedback regulates feedforward retinogeniculate refinement. *Neuron* **91**, 1021–1033 (2016).
- T. Sonoda et al., Experience instructs the refinement of feature selectivity in the mouse primary 6. visual thalamus. Neuron 113, 1352-1362 (2025).
- T. A. Seabrook, R. N. El-Danaf, T. E. Krahe, M. A. Fox, W. Guido, Retinal input regulates the timing of 7 corticogeniculate innervation. J. Neurosci. 33, 10085-10097 (2013).
- J. A. Shanks et al., Corticothalamic axons are essential for retinal ganglion cell axon targeting to the mouse dorsal lateral geniculate nucleus. J. Neurosci. 36, 5252-5263 (2016).
- Y. Diao et al., Reciprocal connections between cortex and thalamus contribute to retinal axon targeting to dorsal lateral geniculate nucleus. Cereb. Cortex 28, 1168-1182 (2018).
- J. W. Phillips et al., A repeated molecular architecture across thalamic pathways. Nat. Neurosci. 22, 1925-1935 (2019).
- R. Cossart, S. Garel, Step by step: Cells with multiple functions in cortical circuit assembly. Nat. Rev. Neurosci. 23, 395-410 (2022).
- 12. D. S. Bortone, S. R. Olsen, M. Scanziani, Translaminar inhibitory cells recruited by layer 6 corticothalamic neurons suppress visual cortex. Neuron 82, 474-485 (2014).
- Y. Liang et al., A distinct population of L6 neurons in mouse V1 mediate cross-callosal communication. Cereb. Cortex 31, 4259-4273 (2021).
- S. N. Tuncdemir et al., Early somatostatin interneuron connectivity mediates the maturation of deep layer cortical circuits. Neuron 89, 521-535 (2016).
- 15 S. J. Wu et al., Cortical somatostatin interneuron subtypes form cell-type-specific circuits. Neuron 111, 2675-2692.e9 (2023).
- H. J. Luhmann, R. Khazipov, Neuronal activity patterns in the developing barrel cortex. Neuroscience 368, 256-267 (2018).
- J. B. Ackman, T. J. Burbridge, M. C. Crair, Retinal waves coordinate patterned activity throughout the developing visual system. Nature 490, 219-225 (2012).
- 18. M. B. Feller, Spontaneous correlated activity in developing neural circuits. Neuron 22, 653-656
- 19. P. Golshani et al., Internally mediated developmental desynchronization of neocortical network activity. J. Neurosci. 29, 10890-10899 (2009).
- N. L. Rochefort et al., Sparsification of neuronal activity in the visual cortex at eye-opening. Proc. 20 Natl. Acad. Sci. U.S.A. 106, 15049–15054 (2009).
- A. Marques-Smith et al., A transient translaminar GABAergic interneuron circuit connects 21. thalamocortical recipient layers in neonatal somatosensory cortex. Neuron 89, 536-549 (2016).
- L. J. Baruchin, F. Ghezzi, M. M. Kohl, S. J. Butt, Contribution of interneuron subtype-specific GABAergic signaling to emergent sensory processing in mouse somatosensory whisker barrel cortex. Cereb. Cortex 32, 2538-2554 (2022).
- L. Modol, M. Moissidis, M. Selten, F. Oozeer, O. Marin, Somatostatin interneurons control the timing of developmental desynchronization in cortical networks. Neuron 112, 2015-2030 (2024).
- L. Modol et al., Assemblies of perisomatic GABAergic neurons in the developing barrel cortex. Neuron 105, 93-105.e4 (2020).
- V. Montero, A quantitative study of synaptic contacts on interneurons and relay cells of the cat lateral geniculate nucleus. Exper. Brain Res. 86, 257-270 (1991).
- R. Guillery, S. M. Sherman, Thalamic relay functions and their role in corticocortical communication: Generalizations from the visual system. Neuron 33, 163-175 (2002).
- F. Briggs, W. M. Usrey, Corticogeniculate feedback and visual processing in the primate. J. Physiol. 27. **589**, 33-40 (2011).
- S. R. Crandall, S. J. Cruikshank, B. W. Connors, A corticothalamic switch: Controlling the thalamus with dynamic synapses. Neuron 86, 768-782 (2015).
- 29. A. Baker et al., Specialized subpopulations of deep-layer pyramidal neurons in the neocortex: Bridging cellular properties to functional consequences. J. Neurosci. 38, 5441-5455 (2018).
- S. C. Feldman, M. R. Harris, L. K. Laemle, The maturation of the somatostatin systems in the rat visual cortex. Peptides 11, 1055-1064 (1990).
- L. Magno et al., Transient developmental imbalance of cortical interneuron subtypes presages longterm changes in behavior. Cell Rep. 35 (2021).
- B. Wamsley et al., Rbfox1 mediates cell-type-specific splicing in cortical interneurons. Neuron 100, 846-859.e7 (2018).
- H. Taniquchi et al., A resource of Cre driver lines for genetic targeting of GABAergic neurons in cerebral cortex. Neuron 71, 995-1013 (2011).
- J. del Rio, L. De Lecea, I. Ferrer, E. Soriano, The development of parvalbumin-immunoreactivity in the neocortex of the mouse. *Dev. Brain Res.* 81, 247–259 (1994).
- 35. X. An et al., A cortical circuit for orchestrating oromanual food manipulation. bioRxiv [Preprint] (2022). https://doi.org/10.1101/2022.12.03.518964 (Accessed 28 March 2025).
- K. S. Matho et al., Genetic dissection of the glutamatergic neuron system in cerebral cortex. Nature **598**, 182-187 (2021).
- B. J. Molyneaux et al., DeCoN: Genome-wide analysis of in vivo transcriptional dynamics during 37 pyramidal neuron fate selection in neocortex. Neuron 85, 275-288 (2015).
- S. J. Wu et al., Pyramidal neurons proportionately alter the identity and survival of specific cortical interneuron subtypes. bioRxiv [Preprint] (2024). https://doi.org/10.1101/2024.07.20.604399 (Accessed 21 July 2024).
- S. Cheng et al., Vision-dependent specification of cell types and function in the developing cortex. Cell 185, 311-327.e24 (2022).
- M. S. Lazarus, Z. J. Huang, Distinct maturation profiles of perisomatic and dendritic targeting GABAergic interneurons in the mouse primary visual cortex during the critical period of ocular dominance plasticity. J. Neurophysiol. 106, 775-787 (2011).

- 41. J. Jaepel, M. Hübener, T. Bonhoeffer, T. Rose, Lateral geniculate neurons projecting to primary visual cortex show ocular dominance plasticity in adult mice. Nat. Neurosci. 20, 1708-1714 (2017).
- J.-P. Sommeijer et al., Thalamic inhibition regulates critical-period plasticity in visual cortex and thalamus. Nat. Neurosci. 20, 1715-1721 (2017).
- H. J. Alitto, W. M. Usrey, Corticothalamic feedback and sensory processing. Curr. Opin. Neurobiol. 13, 440-445 (2003)
- 44. F. Briggs, W. M. Usrey, Emerging views of corticothalamic function. Curr. Opin. Neurobiol. 18, 403-407 (2008).
- S. M. Sherman, Functioning of circuits connecting thalamus and cortex. Compr. Physiol. 7, 713–739 (2011).
- 46. N. J. Miska, L. M. Richter, B. A. Cary, J. Gjorgjieva, G. G. Turrigiano, Sensory experience inversely regulates feedforward and feedback excitation-inhibition ratio in rodent visual cortex. Elife 7, e38846 (2018).
- 47. F. Briggs, Role of feedback connections in central visual processing. Annu. Rev. Vis. Sci. 6, 313-334 (2020).
- 48. B. M. Hooks, C. Chen, Circuitry underlying experience-dependent plasticity in the mouse visual system. Neuron 106, 21-36 (2020).
- F. M. Antunes, M. S. Malmierca, Corticothalamic pathways in auditory processing: Recent advances and insights from other sensory systems. Front. Neural Circuits 15, 721186 (2021).
- 50. M. Fagiolini, T. K. Hensch, Inhibitory threshold for critical-period activation in primary visual cortex. Nature 404, 183-186 (2000).
- T. K. Hensch, Critical period plasticity in local cortical circuits. Nat. Rev. Neurosci. 6, 877-888 (2005).
- Y. Yazaki-Sugiyama, S. Kang, H. Câteau, T. Fukai, T. K. Hensch, Bidirectional plasticity in fast-spiking GABA circuits by visual experience. Nature 462, 218–221 (2009).
- A. E. Takesian, T. K. Hensch, Balancing plasticity/stability across brain development. Prog. Brain Res. 53. 207, 3-34 (2013).
- A. Wang, K. A. Ferguson, J. Gupta, M. J. Higley, J. A. Cardin, Developmental trajectory of cortical somatostatin interneuron function. bioRxiv [Preprint] (2024). https://doi. org/10.1101/2024.03.05.583539 (Accessed 7 March 2024).
- E. A. Phillips, A. R. Hasenstaub, Asymmetric effects of activating and inactivating cortical interneurons. Elife 5, e18383 (2016).
- M. Fagiolini, T. Pizzorusso, N. Berardi, L. Domenici, L. Maffei, Functional postnatal development of the rat primary visual cortex and the role of visual experience: Dark rearing and monocular deprivation. Vision Res. 34, 709-720 (1994).
- L. Benevento, B. Bakkum, R. Cohen, gamma-Aminobutyric acid and somatostatin immunoreactivity in the visual cortex of normal and dark-reared rats. Brain Res. 689, 172-182 (1995).
- B. Morales, S.-Y. Choi, A. Kirkwood, Dark rearing alters the development of GABAergic transmission in visual cortex. J. Neurosci. 22, 8084-8090 (2002).
- L. Gianfranceschi et al., Visual cortex is rescued from the effects of dark rearing by overexpression of BDNF. Proc. Natl. Acad. Sci. U.S.A. 100, 12486-12491 (2003).
- D. Tropea et al., Gene expression changes and molecular pathways mediating activity-dependent plasticity in visual cortex. Nat. Neurosci. 9, 660-668 (2006).
- A. Kreczko, A. Goel, L. Song, H.-K. Lee, Visual deprivation decreases somatic GAD65 puncta number on layer 2/3 pyramidal neurons in mouse visual cortex. Neural Plast. 2009, 415135 (2009).
- J.-P. Sommeijer, C. N. Levelt, Synaptotagmin-2 is a reliable marker for parvalbumin positive inhibitory boutons in the mouse visual cortex. PLoS One 7, e35323 (2012).
- H. Ueno et al., Somatosensory and visual deprivation each decrease the density of parvalbumin neurons and their synapse terminals in the prefrontal cortex and hippocampus of mice. Acta Med. Okayama 67, 135-143 (2013).
- A. van der Bourg et al., Layer-specific refinement of sensory coding in developing mouse barrel cortex. Cereb. Cortex 27, 4835-4850 (2017).
- B. A. Olshausen, D. J. Field, Sparse coding of sensory inputs. Curr. Opin. Neurobiol. 14, 481-487
- L. Madisen et al., A robust and high-throughput Cre reporting and characterization system for the whole mouse brain. Nat. Neurosci. 13, 133-140 (2010).
- L. Madisen et al., A toolbox of Cre-dependent optogenetic transgenic mice for light-induced activation and silencing. Nat. Neurosci. 15, 793 (2012).
- S. Hippenmeyer et al., A developmental switch in the response of DRG neurons to ETS transcription factor signaling. PLoS Biol. 3, e159 (2005).
- E. Y. Litvina, C. Chen, Functional convergence at the retinogeniculate synapse. Neuron 96, 330-338. e5 (2017).
- Q. Jiang et al., Functional convergence of on-off direction-selective ganglion cells in the visual thalamus. Curr. Biol. 32, 3110-3120.e6 (2022).
- R. T. Pressler, W. G. Regehr, Metabotropic glutamate receptors drive global persistent inhibition in the visual thalamus. J. Neurosci. 33, 2494-2506 (2013).
- J. Turner, T. Salt, Characterization of sensory and corticothalamic excitatory inputs to rat thalamocortical neurones in vitro. J. Physiol. 510, 829-843 (1998).
- J. Noutel, Y. K. Hong, B. Leu, E. Kang, C. Chen, Experience-dependent retinogeniculate synapse remodeling is abnormal in MeCP2-deficient mice. Neuron 70, 35-42 (2011).
- A. Kingston et al., LY341495 is a nanomolar potent and selective antagonist of group II metabotropic glutamate receptors. Neuropharmacology 37, 1-12 (1998).
- 75. C. Chen, W. G. Regehr, Developmental remodeling of the retinogeniculate synapse. Neuron 28, 955-966 (2000).
- J. L. Hauser, E. B. Edson, B. M. Hooks, C. Chen, Metabotropic glutamate receptors and glutamate transporters shape transmission at the developing retinogeniculate synapse. J. Neurophysiol. 109, 113-123 (2012).
- J. L. Hauser, X. Liu, E. Y. Litvina, C. Chen, Prolonged synaptic currents increase relay neuron firing at the developing retinogeniculate synapse. J. Neurophysiol. 112, 1714-1728 (2014).
- Y. C. Yang, C. C. Hu, C. S. Huang, P. Y. Chou, Thalamic synaptic transmission of sensory information modulated by synergistic interaction of adenosine and serotonin. J. Neurochem. 128, 852-863
- A. P. Caccavano et al., Divergent opioid-mediated suppression of inhibition between hippocampus and neocortex across species and development. Neuron, 10.1016/j.neuron.2025.03.005 (2025).
- K. C. Allaway et al., Genetic and epigenetic coordination of cortical interneuron development. Nature **597**, 693-697 (2021).